

pH-induced reorientation of cytochrome c on silica nanoparticles

Jens Meissner^a, Yao Wu^b, Jacques Jestin^c, William A. Shelton^{b,d}, Gerhard H. Findenegg^{a,*} and Bhuvnesh Bharti^{b,*}

Received 00th January 20xx,
Accepted 00th January 20xx

DOI: 10.1039/x0xx00000x

www.rsc.org/

The orientation of cytochrome c molecules at the surface of silica nanoparticles was studied in a wide pH range by combining small-angle neutron scattering, adsorption measurements, and molecular dynamics simulations. The results indicate a reorientation of the ellipsoidal protein from head-on to side-on as the pH is increased. This is attributed to changes in the surface charge distribution of both the protein and the nanoparticles.

In the past decade nanomaterials have found their way into numerous biomedical applications, such as *in-vivo* imaging, sensing, and gene therapy.^{1–3} In all these applications, nanosized particles come in direct contact with environments containing many different proteins.⁴ The functionality and biocompatibility of nanomaterials is strongly influenced by their interaction with these proteins. Proteins can adsorb onto nanoparticles through electrostatic, van der Waals, hydrophobic, and/or steric interactions.^{5–9} Several recent studies have been focused on developing a better understanding of these bio-nano interactions.^{10–13} While most of the reports investigate the change in the secondary structure of proteins upon adsorption, less attention has been given to the spatial orientation of the protein at nanoparticles.^{7,14–17} This local orientation on a nanoparticle is decisive for biological activity and functionality of the adsorbed protein.^{18–20} Hence, there is a need to develop new approaches to direct the assembly and local orientation of proteins onto nanocurved surfaces.

The spatial organization of the proteins can be investigated by molecular or atomic probes such as fluorescent dyes and heavy metal ions.^{21–25} However, labelling of proteins with molecular/atomic probes significantly alters the binding energy of the specific site on protein, and cannot provide a measure of protein-substrate interactions.^{24,26} Here we use small angle neutron scattering (SANS) as a non-invasive experimental tool to determine the orientation of proteins at nanocurved interfaces. We combine SANS experiments with molecular dynamic (MD) simulations to identify the local orientation of a model ellipsoidal protein, cytochrome *c* (from horse heart), adsorbed onto silica nanoparticles. We find that the orientation of adsorbed cytochrome *c* is governed by the surface charge distribution on the protein and charge density of the silica surface, which both are altered by changes of pH.

Cytochrome *c* is a small globular protein of 104 amino acid residues covalently bound to a central heme group.^{27,28} It plays a central role in oxygen transport and ATP synthesis in mammals. The isoelectric point (IEP) of cytochrome *c* is at pH 10.7.²⁹ It is widely considered as a “hard” protein which retains its ellipsoid-like shape (2.6 × 3.0 × 3.2 nm) in a wide pH range.³⁰ This is reconfirmed by SANS measurements of cytochrome *c* in the pH range 3–10 (Fig. S1, ESI). Here we investigate the binding and pH induced reorientation of cytochrome *c* on silica nanospheres with diameters of 7 nm, 13 nm and 41 nm, referred to as SiNP7, SiNP13 and SiNP41, respectively. The nanoparticles were synthesized in pure D₂O using previously reported methods^{31,32} and characterized for size and polydispersity by SANS (Fig. S2, Table S1, ESI).

The structure of the protein–nanoparticle complex was determined as a function of pH by SANS experiments on nanoparticle dispersions containing a fixed amount of cytochrome *c*. One such SANS profile for SiNP7 in D₂O containing ~10 cytochrome *c* molecules per nanoparticle at pH 8.3 is shown in Figure 1a. $I(q)$ is the scattering intensity and q is the wave vector given as $q = (4\pi/\lambda)\sin\theta$, where λ is the wavelength of the neutron beam and 2θ is the scattering angle. It should be noted that in pure D₂O, incident neutrons scatter

^a Stranski Laboratory of Physical and Theoretical Chemistry, Technical University Berlin, 10623 Berlin, Germany

^b Cain Department of Chemical Engineering, Louisiana State University, Baton Rouge, LA 70803, USA

^c Laboratoire Léon Brillouin, CEA Saclay 91191 Gif-sur-Yvette Cedex, France

^d Center for Computation and Technology, Louisiana State University, Baton Rouge, LA 70803, USA

* Corresponding email addresses authors:

findenegg@chem.tu-berlin.de

bbharti@lsu.edu

Electronic Supplementary Information (ESI) available: [details of any supplementary information available should be included here]. See DOI: 10.1039/x0xx00000x

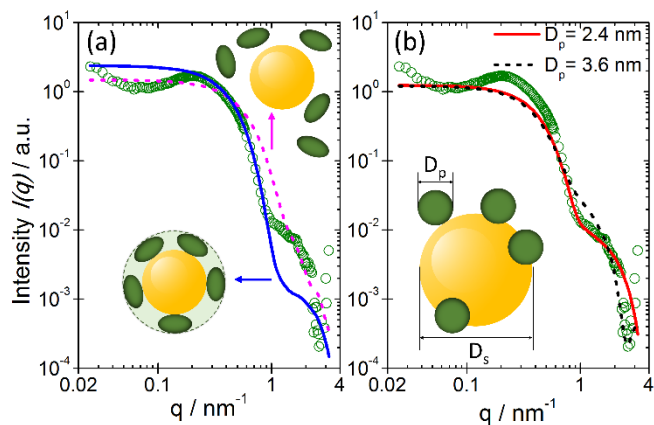


Figure 1 (a-b) SANS profile of mixture of silica nanoparticles (diameter 7 nm) with cytochrome *c* in D_2O . The scattered points are experimental SANS data and lines represent simulated profiles for different protein-silica binding states. The dotted line is the sum of form factors of ellipsoids and spheres representing dispersed protein and nanoparticle respectively. The solid line is the core-shell form factor model representing the silica nanoparticle-protein conjugate. The inset sketches illustrate the conceptual picture of the model used for the respective simulation. The raspberry-like particle model in (b) correctly predicts the high- q scattering of the SANS profile and effective in identifying small changes in the adsorbed protein states.

both from silica and protein, and the scattering profile contains information about the composite structure formed by the silica nanoparticles and cytochrome *c*. The smeared oscillation observed at $q \sim 1 \text{ nm}^{-1}$ is the signature of the form-factor of silica nanoparticles with adsorbed protein. The oscillation at $q \sim 0.2 \text{ nm}^{-1}$ is due to interparticle correlations, i.e. structure factor³¹. Here we determine the structure of the protein-nanoparticle complex and perform a model-dependent analysis of the SANS data in the range $0.3 < q < 3 \text{ nm}^{-1}$.

The applicability of three form-factor models to represent the SANS profiles is tested, namely (a) free spherical nanoparticles with nonadsorbed ellipsoidal protein (Fig. 1a),³³ (b) spherical particles having a uniform shell of protein (Fig. 1a),³³ and (c) discrete protein molecule adsorbed on silica nanoparticles plus nonadsorbed protein (Fig. 1b).³⁴ The models (a) and (b), respectively, overestimate and underestimate the scattering intensity in the range $0.5 < q < 1.5 \text{ nm}^{-1}$, and provide poor representation of the experimental data. The deviations of the two models from the experimental data indicate that the surface area of the nanoscale assembly probed by the neutrons is in-between the cumulative surface area of protein plus nanoparticles, and the surface area of a uniform protein layer formed on the nanoparticles. Such an effect has been reported previously for nonionic surfactants, where discrete surfactant surface micelles rather than a uniform surfactant layer on the nanoparticles gave rise to a similar increase in the scattering intensity at high q .^{33,35}

The total scattering intensity of the protein-nanoparticle dispersion is given as a sum of scattering from nanoparticles with adsorbed protein ("raspberry-like" structure, I_{RB}), and nonadsorbed free protein (I_P), i.e., $I_{total}(q) = I_{RB}(q) + I_P(q)$. From here on this is called RB model. $I_P(q)$ is given as³⁴

$$I_P(q) = \phi_p (1 - \phi_p^a) V_p \Delta \rho_p^2 P_p(q) \quad (1)$$

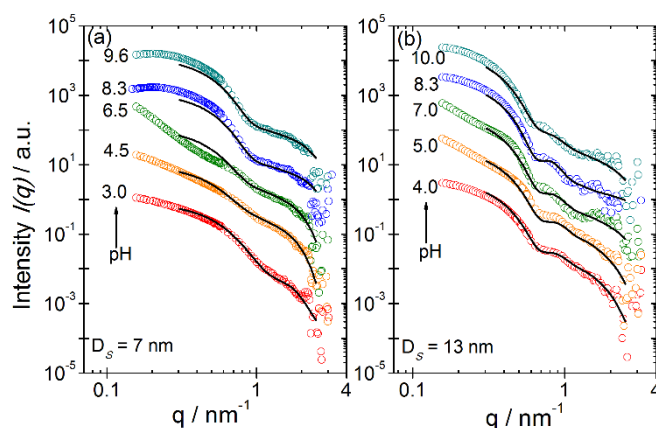


Figure 2. SANS intensity profiles for (a) SiNP7 and (b) SiNP13 particles in D_2O with a fixed amount of cytochrome *c* at different bulk pH values as indicated in the graph. Solid lines represent fits with the RB-model. The curves are shifted by a constant factor of 10 for better visualization.

where ϕ_p is the volume fraction of protein, ϕ_p^a the fraction of protein that is adsorbed at the silica particles, V_p is the volume of a protein molecule, $\Delta \rho_p$ is the scattering length density contrast of protein against the dispersing medium (D_2O), and $P_p(q)$ is the form factor of protein molecules. The scattering intensity from the raspberry-like protein-nanoparticle complex is given as³⁴

$$I_{RB}(q) = \left(\phi_s V_s \Delta \rho_s^2 + 4\chi \phi_p \phi_p^a V_s \Delta \rho_p^2 \frac{D_p}{D_s + D_p} \right) P_{RB}(q) \quad (2)$$

where ϕ_s , V_s , and $\Delta \rho_s$ represent the volume fraction, particle volume, and scattering contrast of the silica particles, D_s and D_p are the diameters of the silica particles and adsorbed protein molecules, χ is the fraction of surface area of the silica particles shadowed by adsorbed protein, and $P_{RB}(q)$ is the form factor of the raspberry-like protein-silica complex as given by eq 10 of ref. 34 (see ESI). Here the adsorbed cytochrome *c* is approximated as a sphere instead of an ellipsoid, and changes in its size (D_p) are attributed to the relative change in local orientation of the adsorbed protein (see later).

Analysis of the experimental SANS profiles shows that the RB-model captures the discrete nature of protein adsorbed on nanoparticles and is sensitive to small changes in the apparent size of adsorbed protein. For example, the SANS profile of SiNP7 with adsorbed protein is represented well by $D_p = 2.4 \text{ nm}$, while $D_p = 3.6 \text{ nm}$ show significant deviations (Fig. 1b).

The RB model is used to analyse experimental SANS profiles for SiNP7, SiNP13 and SiNP41 in the pH range 3-10. The data fitting is performed with only two free fit parameters, namely, protein diameter (D_p) and fraction of surface of silica particles occupied by protein (χ). The model provides an excellent representation of the experimental SANS data in the relevant range $q > 0.5 \text{ nm}^{-1}$ (Fig. 2, Fig. S3, ESI). The deviation of the model predictions from experimental data at $q < 0.5 \text{ nm}^{-1}$ is attributed to the structure factor resulting from protein-bridged nanoparticle aggregates.³² The increase in scattering intensity at $q < 0.5 \text{ nm}^{-1}$ as shown in Fig. 2 and Fig. S3 (ESI) indicate that bridging aggregation is strongly dependent on pH. Large-scale

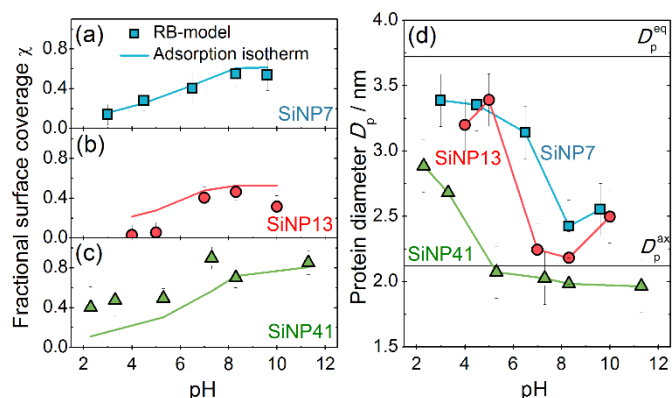


Figure 3. (a–c) Fractional surface of silica nanoparticles occupied by cytochrome *c*, as obtained from the RB-model fitting of the SANS data (points) and independently derived from adsorption isotherms (solid line). (d) Protein diameter as derived from neutron scattering experiments by RB-model fitting for SiNP7, SiNP13 and SiNP41 particles. Solid lines indicate the equatorial (head-on state) and axial (side-on state) diameter of native cytochrome *c* derived from SANS experiments. The decrease in protein size is a signature of flipping of protein from head-on to side-on configuration.

aggregates are formed only in an intermediate pH range (pH 5–7), in which high values of the fractal dimension n are extracted from the slope of the scattering intensity profiles, $I(q) \propto q^{-n}$, while only small aggregates prevail at pH values outside this range. This aspect of nanoparticle aggregation has been investigated extensively in previous reports.^{28,31} We recognize that the orientation of protein molecules may be impacted by the nanoparticle aggregation. However, this effect will be small, as geometric packing considerations show that only a small fraction of the adsorbed protein molecules is forming bridges between nanoparticles while the large majority is not involved in bridging. Further details on this aggregation aspect can be found elsewhere.^{31,32}

The fraction of surface of the nanoparticles occupied by the protein (χ) as derived by fitting the RB model to the SANS data is shown in Figure 3a–c (Tables S3, S4, ESI). The observed increase in χ with pH agrees with results of independent adsorption measurements (Fig. S4, ESI). Adsorption remains well below a densely packed monolayer, hence strong correlations in the layer of adsorbed protein can be excluded, which would limit the applicability of this model. The agreement between the prediction of the RB model and adsorption data represents strong support for the suitability of this model to predict the local characteristics of bound protein. The observed increase in adsorption of protein onto silica nanoparticles with growing pH is attributed to the increasing electrostatic interaction of positively charged cytochrome *c* with the increasingly negative silica surface.²⁸ On the other hand, at low pH the observed binding of highly charged protein to weakly charged silica is the result of “protein-halo” formation on the nanoparticle. This halo formation is attributed to the charge-charge repulsions between protein molecules in bulk, as presented previously.^{36–38}

The effective diameter of adsorbed protein molecules as determined by fitting the RB model to the SANS profiles decreases with increasing pH, namely from 3.4 nm at acidic pH to 2.3–2.5 nm at neutral and basic pH for SiNP7 and SiNP13, and from 2.9 nm to 2.2–2.0 nm for SiNP41 (Fig. 3d). Importantly, no pH dependent size change of cytochrome *c* is observed in the absence of the silica (Fig.

S1, ESI). We attribute this apparent decrease in D_p to a change in orientation of the protein from a “head-on” to a “side-on” configuration. This transition takes place in pH range 3–7 in which the net charge of cytochrome *c* strongly decreases with increasing pH.²⁸ There is also a systematic shift of this transition to lower pH as the particle size increases (Fig. 3d). This trend in the reconfiguration pH-range is attributed to the effect of local curvature of the nanoparticles, where increasing curvature leads to weaker attraction between the binding sites of silica nanoparticles and adsorbing species.

To gain insight into the origin of the reorientation of protein on

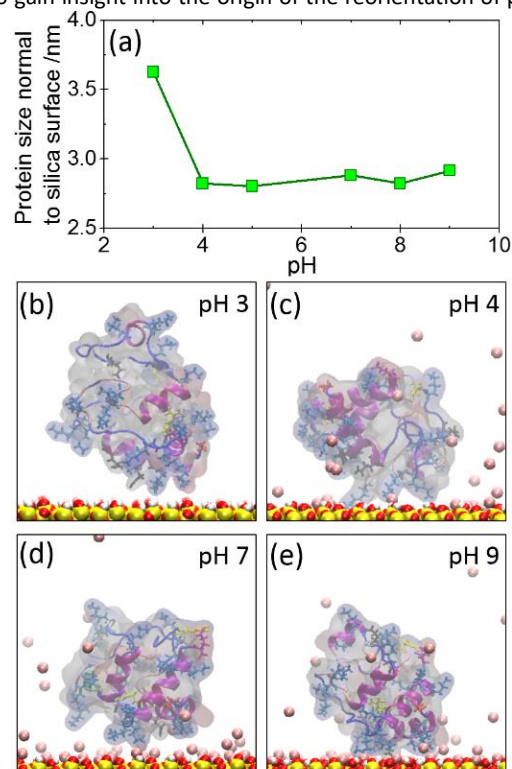


Figure 4. (a) End-to-end distance of adsorbed cytochrome *c* orthogonal to the silica surface as determined by MD simulations. (b–e) Equilibrium adsorption state of cytochrome *c* on SiNP41 surface at increasing pH. The morphology of cytochrome *c* molecule is shown highlighted by a ghost surface.

silica nanoparticles, the pH induced change in the surface charge distribution on cytochrome *c* was estimated by molecular dynamics (MD) simulations in the NVT ensemble at 300 K. Simulations were performed with the NAMD 2.9 package³⁹ using the CHARMM-SILICA⁴⁰ force-field and analysed using VMD.⁴¹ In all simulations the initial protein orientation was the same, with the centre of mass 3.4 nm away from the silica surface (Fig. S5, Movie S1). Attachment to the surface in a stable configuration was achieved within 100 ns regardless of pH value.

Our simulations show that the adsorption of cytochrome *c* occurs via positively charged amino acid residues binding to negatively charged silica surface. At pH 3, the silica surface is weakly ionized and the binding of protein is dominated by the discrete charges at the surface. The sparsely distributed charged sites on silica drives the adsorption of the ellipsoidal protein with only two amino acid residues (Lys8 and Lys5) of the cytochrome *c* (Fig. 4b). At higher pH, the number of siloxide

groups ($\equiv\text{SiO}^-\text{Na}^+$) increases and the protein binding occurs via multiple charged sites. The increasing number of binding sites on silica drives the adsorption of protein via multiple charged amino acid residues and thus reorients cytochrome *c* from head-on to a side-on adsorbed state. The simulations show that the adsorption of cytochrome *c* to silica surface at pH 7 occurs via five amino acid residues, namely Lys87, Lys86, Gln16, Lys79, and Lys8 (Fig. S6, ESI).

The reorientation of the adsorbed cytochrome *c* observed in the simulations is quantified by measuring its end-to-end distance normal to the silica surface (Fig. 4a). This “effective size” of the protein at the silica surface decreases sharply from pH 3 to pH 4, in agreement with the behaviour observed by the SANS data analysis (Fig. 3d).

Preferential binding of protein via its positive patches has been shown experimentally for human carbonic anhydrase and simulated for lysozyme on amorphous silica surfaces^{17,25}. The orientation of cytochrome *c* on a planar electrode was shown to be affected by the interfacial potential during the adsorption process⁴². Here, we find that a similar relationship exists between the surface charge distribution and local orientation of cytochrome *c* on nanosilica, but with a strong pH and particle-curvature dependence. The pH induces a charge redistribution on cytochrome *c* and increases the charge density on silica nanoparticles, which further drives a rearrangement of amino acid residues preferentially binding to silica and induces protein reorientation. An increase in the curvature of nanoparticle causes an increase in the pH at which cytochrome *c* flips from head-on to side-on state. This shift of reorientation pH is attributed to the decrease in net attraction between the silica surface and protein upon increasing the curvature. The study presents a basis for understanding the variations in biological activity of discrete protein molecules adsorbed on surfaces at different pH and curvatures, thus enabling a design-principle of nanomaterial fabrication for biomedical applications.

Conclusions

In conclusion, a combination of SANS and MD simulations is used to discover the role of pH and surface curvature on the orientation of cytochrome *c* on silica nanoparticles. Raspberry-like particle model is used to analyse the experimental SANS profiles in the pH range 2–10. The SANS experiments and MD simulations both show that at pH < 4 the protein adsorbs with a head-on configuration, but with increasing pH a reorientation to a side-on orientation takes place. This reorientation is caused by a change in surface electrostatic interactions between silica and cytochrome *c*, which further alters the amino acid residues binding to nanoparticles. These results provide a new insight into the effect of pH on the protein binding and orientation onto nanoparticles, which may play an important role in biological activity of the adsorbed protein. An ability to control the orientation of protein on nanoparticles will have a direct impact on the development functional materials enabling purification of antibodies, and modulating enzymatic activity of the adsorbed protein^{18–20}. The study presented here provides a better understanding of bio-nano interactions, which not only

help in further development of new platforms for advanced biomedical applications, but may also lead to new paradigms for the directed interfacial assembly of proteins with the desired functionality.

Conflicts of interest

There are no conflicts to declare.

Notes and references

‡ Footnotes relating to the main text should appear here. These might include comments relevant to but not central to the matter under discussion, limited experimental and spectral data, and crystallographic data.

Acknowledgements

Authors thank Prof. O. D. Velev (NCSSU), Prof. M. Gradzielski (TU Berlin) for useful discussions, and Dr. Zhenyu Di for assistance with the SANS measurement at FRM II. This material is based upon work supported by the U.S. Department of Energy, Office of Science, Basic Energy Sciences, under EPSCoR Grant No. DE-SC0012432 with additional support from the Louisiana Board of Regents, and the Deutsche Forschungsgemeinschaft (IRTG-1524).

References

1. E. C. Dreaden, A. M. Alkilany, X. Huang, C. J. Murphy, and M. A. El-Sayed, *Chem. Soc. Rev.*, 2012, **41**, 2740–2779.
2. J. J. Giner-Casares, M. Henriksen-Lacey, M. Coronado-Puchau, and L. M. Liz-Marzán, *Mater. Today*, 2016, **19**, 19–28.
3. A.-C. Genix and J. Oberdisse, *Soft Matter*, 2018, **14**, 5161–5179.
4. R. A. Yokel and R. C. MacPhail, *J. Occup. Med. Toxicol.*, 2011, **6**, 7.
5. T. MičlÁuř, C. Beer, J. Chevallier, C. Scavenius, V. E. Bochenkov, J. J. Enghild, and D. S. Sutherland, *Nat. Commun.*, 2016, **7**, 1–10.
6. M. Rabe, D. Verdes, and S. Seeger, *Adv. Colloid Interface Sci.*, 2011, **162**, 87–106.
7. P. Roach, D. Farrar, and C. C. Perry, *J. Am. Chem. Soc.*, 2005, **127**, 8168–8173.
8. S. Gon and M. M. Santore, *Langmuir*, 2011, **27**, 1487–1493.
9. M. M. Santore and C. F. Wertz, *Langmuir*, 2005, **21**, 10172–10178.
10. J. Hladílková, T. H. Callisen, and M. Lund, *J. Phys. Chem. B*, 2016, **120**, 3303–3310.
11. F. Ding, S. Radic, R. Chen, P. Chen, N. K. Geitner, J. M. Brown, and P. C. Ke, *Nanoscale*, 2013, **5**, 9162–9169.
12. A. Kondo, S. Oku, and K. Higashitani, *J. Colloid Interface Sci.*, 1991, **143**, 214–221.
13. F. Liu, L. Xue, Y. Yuan, J. Pan, C. Zhang, H. Wang, J. L. Brash, L. Yuan, and H. Chen, *Nanoscale*, 2016, **8**, 4387–4394.
14. W. Shang, J. H. Nuffer, V. A. Muñiz-Papandrea, W. Colón, R.

- W. Siegel, and J. S. Dordick, *Small*, 2009, **5**, 470–476.
15. P. Roach, D. Farrar, and C. C. Perry, *J. Am. Chem. Soc.*, 2006, **128**, 3939–3945.
16. S. M. Daly, T. M. Przybycien, and R. D. Tilton, *Langmuir*, 2003, **19**, 3848–3857.
17. N. Hildebrand, S. Köppen, L. Derr, K. Li, M. Koleini, K. Rezwan, and L. Colombi Ciacchi, *J. Phys. Chem. C*, 2015, **119**, 7295–7307.
18. S. Kim, D. Sung, and J. H. Chang, *Medchemcomm*, 2018, **9**, 108–112.
19. T. W. Cha, A. Quo, and X. Y. Zhu, *Proteomics*, 2005, **5**, 416–419.
20. F. Liu, L. Wang, H. Wang, L. Yuan, J. Li, J. L. Brash, and H. Chen, *ACS Appl. Mater. Interfaces*, 2015, **7**, 3717–3724.
21. C. Nitsche and G. Otting, *Prog. Nucl. Magn. Reson. Spectrosc.*, 2017, **98–99**, 20–49.
22. D. Marion, *Mol. Cell. Proteomics*, 2013, **12**, 3006–3025.
23. X. Chen, R. Ferrigno, J. Yang, and G. M. Whitesides, *Langmuir*, 2002, **18**, 7009–7015.
24. J. Romanowska, D. B. Kokh, and R. C. Wade, *Nano Lett.*, 2015, **15**, 7508–7513.
25. M. Karlsson and U. Carlsson, *Biophys. J.*, 2005, **88**, 3536–3544.
26. C. P. Toseland, *J. Chem. Biol.*, 2013, **6**, 85–95.
27. A. Hung, S. Mwenifumbo, M. Mager, J. J. Kuna, F. Stellacci, I. Yarovsky, and M. M. Stevens, *J. Am. Chem. Soc.*, 2011, **133**, 1438–1450.
28. B. Bharti and G. H. G. H. Findenegg, *Chem. Lett.*, 2012, **41**, 1122–1124.
29. S. T. Moerz and P. Huber, *J. Phys. Chem. C*, 2015, **119**, 27072–27079.
30. P. Baglioni, E. Fratini, B. Lonetti, and S. H. Chen, *J. Phys. Condens. Matter*, 2004, **16**.
31. B. Bharti, J. Meissner, and G. H. Findenegg, *Langmuir*, 2011, **27**, 9823–9833.
32. B. Bharti, J. Meissner, S. H. L. Klapp, and G. H. Findenegg, *Soft Matter*, 2014, **10**, 718–728.
33. B. Bharti, J. Meissner, U. Gasser, and G. H. Findenegg, *Soft Matter*, 2012, **8**, 6573–6581.
34. K. Larson-Smith, A. Jackson, and D. C. Pozzo, *J. Colloid Interface Sci.*, 2010, **343**, 36–41.
35. D. M. Lugo, J. Oberdisse, A. Lapp, and G. H. Findenegg, *J. Phys. Chem. B*, 2010, **114**, 4183–4191.
36. V. Tohver, J. E. Smay, A. Braem, P. V. Braun, and J. A. Lewis, *Proc. Natl. Acad. Sci.*, 2001, **98**, 8950–8954.
37. F. Zhang, G. G. Long, P. R. Jemian, J. Ilavsky, V. T. Milam, and J. A. Lewis, *Langmuir*, 2008, **24**, 6504–6508.
38. X. Xing, G. Sun, Z. Li, and T. Ngai, *Langmuir*, 2012, **28**, 16022–16028.
39. J. C. Phillips, R. Braun, W. Wang, J. Gumbart, E. Tajkhorshid, E. Villa, C. Chipot, R. D. Skeel, L. Kalé, and K. Schulten, *J. Comput. Chem.*, 2005, **26**, 1781–1802.
40. F. S. Emami, V. Puddu, R. J. Berry, V. Varshney, S. V. Patwardhan, C. C. Perry, and H. Heinz, *Chem. Mater.*, 2014, **26**, 2647–2658.
41. W. Humphrey, A. Dalke, and K. Schulten, *J. Mol. Graph.*, 1996, **14**, 33–38.
42. V. Hitaishi, R. Clement, N. Bourassin, M. Baaden, A. de Poulpiquet, S. Sacquin-Mora, A. Ciaccafava, and E. Lojou, *Catalysts*, 2018, **8**, 192.